Design and performance evaluation of a high power density EMI filter for PWM inverter-fed induction motor drives

G. Ala, G. C. Giaconia, G. Giglia
Dipartimento di Energia, Ingegneria dell'Informazione e Modelli Matematici
Università degli Studi di Palermo
Viale delle Scienze - 90128 Palermo, ITALY
e-mail: guido.ala@unipa.it, costantino.giaconia@unipa.it, graziella.giglia@unipa.it

M. C. Di Piazza, G. Vitale
Istituto di Studi sui Sistemi Intelligenti per l'Automazione
Consiglio Nazionale delle Ricerche
via Dante,12 - 90141 Palermo, ITALY
e-mail: dipiazza@pa.issia.cnr.it, vitale@pa.issia.cnr.it

***Abstract*—This paper presents the design of an electromagnetic interference (EMI) filter for a low voltage high current induction motor drives supplied by DC power grids. In order to effectively design the EMI filter a suitable common mode/differential mode (CM/DM) separation technique has been used. Due to the high operating currents, the software based separation technique using time domain measurements has been applied. The proposed technique allows the CM and DM sections of the EMI filter to be properly selected in a more economical way, i.e. without the need of dedicated hardware or costly radio frequency (RF) instrumentation. The design has been done according to a power density criterion. The effectiveness of the proposed CM/DM separation technique and the EMI filter features/performance have been assessed by experimental tests, carried out with a 1.1 kW PWM inverter-fed induction motor drive, supplied by a 48V DC power grid.**

***Index Terms*— CM and DM separation techniques; EMI filter; Motor drives; Power Converters; Power Density.**

I. INTRODUCTION

Due to the high-speed switching operation, power electronic converters are potential sources of relevant electromagnetic interference (EMI) for equipment placed nearby [1-2].

Technical literature provides a large number of contributions concerning the reduction of electromagnetic noise generated at the output or the input of PWM inverters in induction motor drives. In particular, the methods proposed in scientific literature range from the selection of appropriate inverters switching patterns to the use of passive or active filter-based solutions [3]-[7]. Since EMI filters usually account for as much as 30% of the total converter weight, the aspect of power density, i.e. the amount of managed power per volume unit, is of pivotal importance. As a consequence, the reduction of the EMI filter size has become a key design goal for power electronic equipment, especially in vehicle applications where compactness and low weight are primary issues. Several techniques have been proposed to obtain a good power density-oriented design of EMI filters for power electronic converters. They are mainly based on the realization of compact layouts obtained for example by using suitable winding structures and high performance magnetic materials for the inductance cores [8]. The use of planar structures for realizing both the inductive and capacitive part of the so called integrated EMI filter is one of the most recent technology. In addition, the integrated EMI filter structure has been proposed as well in several power converter scheme in a power range up to hundreds of watt [9]. On the other hand, very few contributions are present in technical literature as far as the power density based design of an EMI filter for inverter-fed induction motor drives is concerned [10]. In particular, no previous examples referred to low voltage high current induction motor drives have been discussed.

In this paper a high power density EMI filter design procedure for low voltage-high current induction motor drives intended for vehicle applications is presented. The design procedure uses a well-known software-based common mode/differential mode (CM/DM) mode separation technique to design an effective EMI filter avoiding dedicated hardware or costly radio frequency (RF) instrumentation, which is particularly critical due to the high values operating currents; here the advantages of this technique with regard to power density design issues are highlighted. CM and DM separation techniques can be roughly classified into three main groups: RF measurement-based, separation techniques based on the use of additional dedicated networks and software-based techniques [11]-[14]. The separation of CM and DM EMI by using a RF current probe [11] and a spectrum analyzer is a very reliable technique; on the other hand, in kW-low voltage applications, the use of RF current probes of suitable ratings are needed to avoid saturation or sensitivity problems, thus implying a significant cost. The use of hardware separators (e.g., Paul Hardin separators, power combiners, etc.) may give phase coherency problems and results degradation without a good characterization of the unavoidable modal conversion of the complete set-up (i.e. the measured level at the DM output in case of pure CM excitation and vice-versa). Moreover the EMI separators are suitable for low-medium power levels, due to the saturation of their wideband transformer [12]. Software-based separation techniques using time domain measurements are generally considered as easy and cost-effective methods for designing the EMI filters, provided that a multi-port digital oscilloscope with suitable sampling capability is available. Moreover, these techniques can reduce the phase coherency problems without any dedicated hardware.

In software-based CM and DM noise separation techniques for conducted EMI, CM and DM signals are acquired in time domain and their frequency spectra are computed using a software-based post-processing. In particular Welch and Bartlett periodograms are proposed in [13] to represent the frequency spectra of CM and DM noise. In [14] a Labview-based measurement system is used. Both contributions state the advantage of the technique and show a qualitative comparison with RF measurement-based separation techniques in the case of low power switched mode power supplies (SMPSs); on the other hand, the difference between CM and DM mode obtained by the different techniques is not quantified.

The CM/DM separation technique used in this paper is based on contemporaneous time domain measurements of CM and DM noise by a multi-channel digital oscilloscope, and the use of a discrete fast Fourier transform (DFFT) computation algorithm, as a post processing technique. The results obtained with the proposed technique have been compared with those found by using a high bandwidth RF current probe and a spectrum analyzer. Differently from other contributions in technical literature, difference between the results obtained by the two techniques, has been evaluated in terms of normalized root mean square error and normalized average. The consolidated technique has been simplified, in particular no window function has been considered in the algorithm since repeated measurements have shown no significant variation in the noise profiles. The use of the DFFT instead of Bartlett/Welch periodograms allows to avoid the need of appropriate margins to compensate the reduction of signal spectra amplitude during the filter design. The use of such a separation technique implies the use of instantaneous common mode current (I_{cm}) and differential mode current (I_{dm}) measurements. These last quantities are very useful for the appropriate choice of the magnetic core for the CM choke, since they allow to evaluate the maximum value of the magnetic induction in the core and to assess saturation issues as well. Therefore, the chosen separation technique is to be considered the most suitable also with regard to the optimal design in terms of power density of the CM choke, which is the bulkiest part of the overall EMI filter. Once the effectiveness of the separation technique has been proven, the evaluated CM and DM noise levels have been used to design the EMI filter for the PWM inverter fed induction motor drive under study. According to a high power density concept [15], the filter has been built up by using a high permeability magnetic material for the CM choke, which allows the overall volume and weight to be reduced respect to the case of using a conventional ferrite core. Finally, experimental tests have been executed to verify the EMI filter performance.

II. Case Study Test Bench

PWM inverter-fed induction motor drives supplied by a DC power grid are used in a broad variety of applications, i.e., vehicle applications (road vehicles, marine vehicles, aircrafts) and can be simply operated in a DC distribution system, such as in the case of some DC distribution micro-grids for residential/commercial smart buildings [16]. For this reason, such a motor drive scheme has been chosen as case study. The test bench is composed as follows. A PWM IGBT Voltage Source Inverter (VSI), equipped with a STGIPS10K60A module; an Altera Cyclone III FPGA board equipped with a Nial Stewart GPIB expansion board, implementing the PWM modulator; a 48V induction motor with a rated power of 1.1 kW. The VSI switching frequency is equal to 20 kHz. The use of an intelligent module for the VSI allows a very compact layout of the power electronic stage. Fig. 1 shows the experimental arrangement of the drive under study. A dual DC Line Impedance stabilization Network (LISN) with a voltage capability up to 600V has been set-up and used to measure the conducted EMI.

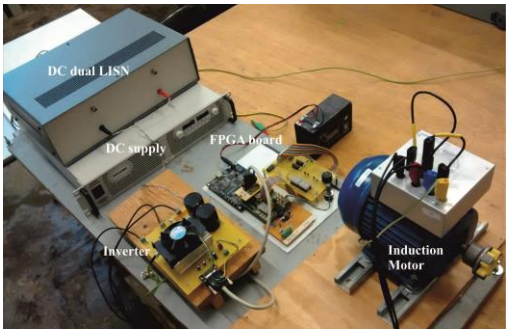

Fig. 1. View of the PWM induction motor drive.

III. EMI Filter General Design Procedure

As well established, the conducted electromagnetic emission can be decomposed in DM and CM noise. The generation and coupling mechanisms as well as the CM and DM EMI paths are different and therefore separated filter sections are needed in order to obtain suitable attenuation for EMC compliance. Both CM and DM filter components are usually embedded into a single filter topology; therefore, it is necessary to separately evaluate the two noise modes as a basic step to design an effective EMI filter [7]. The general topology of an EMI filter used to attenuate the CM and DM noise is shown in Fig. 2. The filter is composed of passive components acting on CM or DM noise separately, and other elements simultaneously affecting both types of noise.

The capacitors C_y attenuate both CM and DM noise and they are generally in the order of magnitude of nF; their value is very small compared to that of C_{x1} and C_{x2}, which are in the µF range, so their effect on the DM noise is almost negligible. On the other hand, the capacitor C_x between the electrical lines only attenuates the DM noise. The bulkiest component of the filter is the common mode choke, L_{CM}, that ideally suppresses only the CM noise; however its leakage inductance ($L_{leakage}$) is usually sufficient to attenuate the DM noise as well [17]. Sometimes an additional inductance in series with the L_{CM} (L_{DM_extra}) might be useful to increase the total value of the DM inductance. The procedure followed in designing the CM and DM filter components is described below.

The first step is the identification of the crucial point on the experimental curve of the EMI emission, i.e., the emission peak at the lowest frequency. Therefore it is necessary to measure the CM and DM components

separately and to obtain their frequency spectra as the initial step of the design procedure. The required attenuation for the CM e DM noise are calculated as follows, (1) and (2).

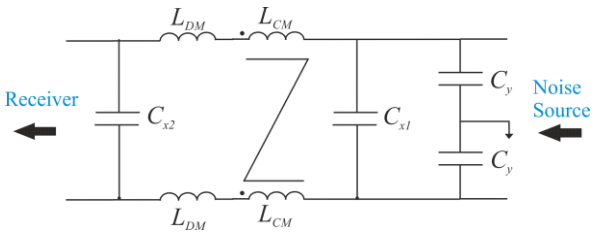

Fig. 2. Generic topology of the EMI filter.

$$A_{req\_att\_CM}[dB\mu V] = A_{h\_att\_CM}[dB\mu V] - Limit[dB\mu V] + 6dB\mu V \quad (1)$$

$$A_{req\_att\_DM}[dB\mu V] = A_{h\_att\_DM}[dB\mu V] - Limit[dB\mu V] + 6dB\mu V \quad (2)$$

where A_{h_att} is the amplitude of the harmonic to be attenuated, *Limit* is the maximum amplitude allowed by the reference standard at the frequency of interest and *6 dBμV* specifies an additional safety margin.
The cut-off frequency of the CM or DM filter, for CM or DM, is given by (3):

$$f_{o\_CM/DM} = \frac{f_{h\_att}}{10^{\frac{A_{req\_att}}{filt\_att}}} \quad (3)$$

where f_{h_att} is the harmonic frequency to be attenuated and *filt_att* is the filter intrinsic attenuation [17].

The f_o value, obtained by (3), should be lower than the converter switching frequency value (f_{PWM}) in order to improve the filter performance and to avoid possible amplification of the switching frequency harmonics. When both the corner frequencies are known, the inductors and capacitors values are determined, according to (4)-(6).

$$L_{CM} = \frac{1}{C_{CM}(2\pi f_{o\_CM})^2} \quad C_{CM} = 2C_Y \quad (4)$$

$$L_{DM} = (0.1 \div 2)\% L_{CM} \quad (5)$$

$$C_{DM} = C_{x1} = C_{x2} = \frac{1}{L_{DM}(2\pi f_{o\_DM})^2} \quad (6)$$

Since as for the DM inductance the leakage inductance of the CM choke is generally used, it is approximated to 0.1-2% of the CM choke inductance value, depending on the core material [4].

IV. CM/DM Separation Technique

The chosen software-based CM/DM separation technique is described in subsection *A*, whereas the RF measurement based technique, used as a reference to evaluate the effectiveness of the proposed method, is illustrated in subsection *B*.

A. The proposed software based separation technique

The signals on the phase and neutral conductors of the dual LISN, are simultaneously measured by a multi-channel Digital Storage Oscilloscope (DSO) with a high sampling frequency. Considering that the signals retrieved from CH1 (U_1) and CH2 (U_2) are tied to DM and CM voltages U_{DM} and U_{CM}, referring to Fig. 3, by relationships in (7) and (8), respectively,

$$2U_{DM} = U_1 - U_2 \quad (7)$$

$$2U_{CM} = U_1 + U_2 \quad (8)$$

their separation can be achieved in time domain by simply summing and subtracting the measured signals. This operation is done by using the DSO processing features.

The concurrent signals measurement guarantees phase coherency; the high sampling frequency/processing speed of the instrument and the suitability of time domain signals to be processed by a DFFT algorithm enables to obtain an accurate frequency spectrum of the CM and DM EMI in the range 150 kHz - 30 MHz. In particular, according to the Nyquist-Shannon sampling theorem [18], the DSO sampling rate should be at least two times that of the highest signal frequency. The DFFT algorithm can be simply executed on a PC or implemented on an embedded system as a part of an automated tool for EMI filter design. An accurate time triggering of the signals is done with the aim of capturing an integer number of the PWM switching periods. Moreover the DSO sampling rate and the length of measurement should be chosen so that the resulting resolution of the DFFT is the same of the RF based measurements. In this way the DFFT results can be directly compared with the RF measurements without the need of windowing techniques, used to reduce spectral leakage issues. In this way a simplification is obtained in the subsequent phase of EMI filter design since the use of appropriate margins to compensate the reduction of signal spectra amplitude due to windowing can be avoided. Fig. 3 shows a block diagram, synthesizing the software based CM/DM separation technique concept.

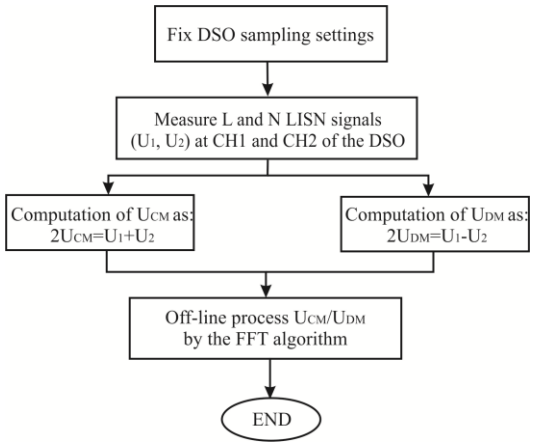

Fig. 3. Block diagram of the time domain EMI measurement method.

B. *Separation technique with current probes*

A RF measurement technique has been used as a reference methodology to benchmark the proposed software-based CM/DM separation method.

The RF separation method is based on the use of a high bandwidth current probe to measure, via spectrum analyzer, the CM and DM noise between the LISN and the disturbance source. It should be considered that, during the tests, the RF current probe is exposed to the typically high supply current. Therefore saturation or sensitivity problems should be taken into account in the choice of a suitable current probe, especially in high power-low voltage applications, such as that considered in this study.

In addition, since the actual impedance of the LISN is not strictly constant within the frequency range of the conducted EMI, a suitable frequency-dependent conversion factor, corresponding to the CM and DM LISN impedance, has to be taken into account in order to obtain an accurate measurement of the desired CM and DM voltages. The measuring principle is shown in Fig. 4.

The spectrum analyzer (or EMI test receiver), connected to the current probe, measures twice the CM current and twice the DM current depending on the wire placement respect to the probe. The EMI instrument measures the voltage over a 50Ω resistor and scales it according to (9).

$$EMI\left[dB(\mu V)\right] = 20 \cdot \log U + 120 \qquad (9)$$

In order to obtain the current level in dB(μA) it is necessary to add the correction factor *k* of the current probe to the voltage level in dB(μV):

$$I\left[dB(\mu A)\right] = U\left[dB(\mu V)\right] + k\left[dB\left(\frac{V}{A}\right)\right] \qquad (10)$$

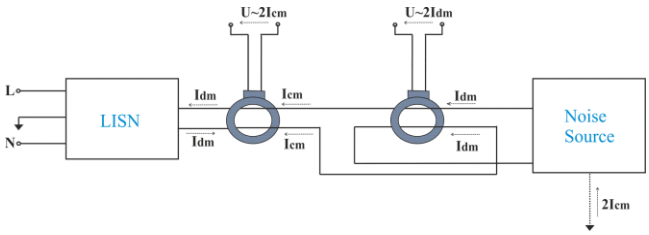

Fig. 4. Separation of CM and DM current by using a current probe.

As well established, the LISN ideally provides a 50Ω load (per power wire) for the conducted EMI in the frequency range between 150 kHz and 30 MHz. As already underlined, the CM and DM LISN impedance values may be subjected to some variations, as shown in Fig. 5, in which the CM and DM measured LISN impedance are reported. Therefore, in order to obtain a more accurate evaluation of the CM/DM noise, the real impedance values $Z_{CM\_LISN}(f)$ and $Z_{DM\_LISN}(f)$ at different frequencies, obtained by a precision LCR meter, must be used. Then:

$$EMI_{CM} = 20 \cdot \log I_{CM} + 20 \cdot \log Z_{CM\_LISN}(f) \qquad (11)$$

$$EMI_{DM} = 20 \cdot \log I_{DM} + 20 \cdot \log Z_{DM\_LISN}(f) \qquad (12)$$

V. Experimental Validation of the Software-Based CM/DM Separation

The effectiveness of the software-based CM/DM separation technique has been verified by comparing the results with those obtained by the RF measurement-based CM/DM separation technique described in section IV.*B*. The test bench shown in Fig. 1 has been used.

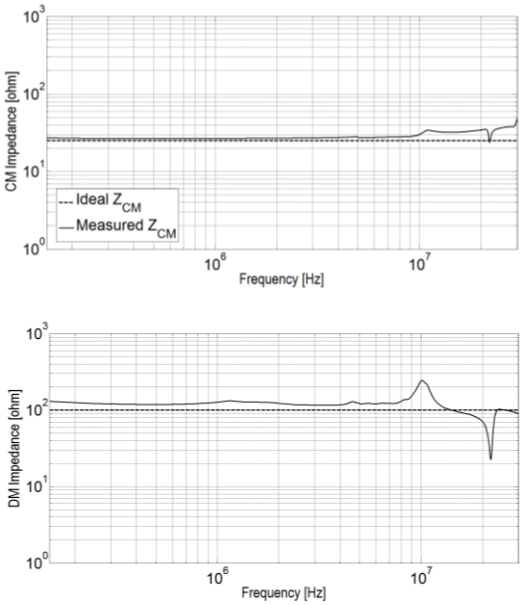

Fig. 5. Comparison between the ideal and measured CM (upper) and DM (lower) LISN impedance.

In particular, a Tektronix TDS7254B 2,5GHz - 20GS/s - 4 channels is used for the time domain measurements needed for the software-based CM/DM separation technique. A RF current probe R&S EZ-17 that allows measurements in the frequency range 20Hz-100MHz with a maximum DC current of 300A, and an Agilent E4402 (9 kHz-3GHZ) spectrum analyzer have been employed for the RF measurement-based separation technique. A 10 kHz resolution has been chosen for both the measurement instruments to obtain directly comparable frequency spectra. Figs. 6 and 7 show the comparison between CM and DM EMI obtained with the separation techniques described in sections IV.*A* and IV.*B*, respectively. It is possible to observe that the obtained results are very close to each other. To quantify the difference of the software-based method results respect to the RF measurement-based ones, the normalized root mean square error (NRMSE) and the normalized average error (NAVE) have been considered over the considered frequency range [19].

Such indices have been normalized with respect to the maximum amplitude of the RF measured emission and they give a quantitative evaluation of the proposed technique performance. Table I summarizes the obtained performance indices. The low values of the performance indices demonstrate the goodness of the software based separation

technique and allows to consider it as a valid tool for the noise mode separation in cases where high operating currents make critical the use of other methods.

TABLE I.
PERFORMANCE INDICES.

Noise Mode	NRMSE (%)	NAVE (%)
CM	13.3	0.28
DM	2.3	0.24

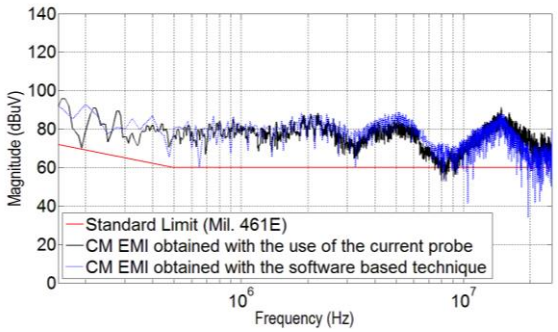

Fig. 6. Comparison between CM EMI obtained by the software-based separation technique and by RF measurement-based technique.

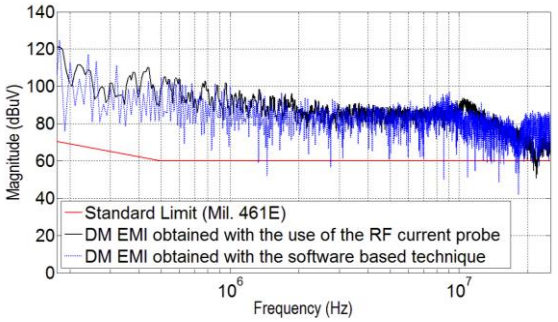

Fig. 7. Comparison between DM EMI obtained by the software-based separation technique and by RF measurement-based technique.

VI. EMI FILTER DESIGN, REALIZATION AND PERFORMANCE

A. *General design issues*

As shown in Figs. 6 and 7, both the CM and DM emission exceeds the Mil 461 E standard limit [20], chosen as a reference. This calls for a suitable input EMI filtering. On the basis of the design procedure described in section III, an EMI filter has been set up and the following input data have been used for the design procedure: CM emission peak at the lowest frequency: 93dBµV@200kHz; DM emission peak at the lowest frequency: 124dBµV@180kHz; cut-off frequencies f_{o_CM}=12.5 kHz and f_{o_DM}= 18 kHz; C_{CM}=200 nF (maximum value allowed according to SAE AS 1831 Standard) [21].

The criterion of a compact CM choke realization has been followed to increase the power density of the EMI filter. To this aim a highly performing magnetic material8 has been chosen for the CM choke core. Nanocrystalline cores from Vacuumschmelze GmbH (VAC) has been considered as the best choice due to their high permeability, resulting in a high inductance/volume ratio, and excellent high-frequency behavior.

In particular, the VITROPERM 500F material has been used; its magnetic performance are significantly higher than those of commonly adopted ferrite and amorphous materials. The nanocrystalline material ensures minimal eddy current losses [22] and in this case the leakage of the CM choke is assumed to be 0.2%. Fig. 8 shows the comparison between magnetization characteristics and magnetic permeability versus frequency curves of the VITROPERM 500F and of a typical Mn-Zn ferrite. Table II gives the comparison between the main geometrical and magnetic characteristics of a N30 ferrite core and a VITROPERM core suited to realize the required CM choke inductance. The very high values of the magnetic permeability/section core ratio (A_L) and saturation flux density (B_{sat}) of nanocrystalline materials allow to obtain very high inductance values with reduced section of the core and number of turns. This leads also to low copper losses and small winding capacitance which gives improved high frequency performance.

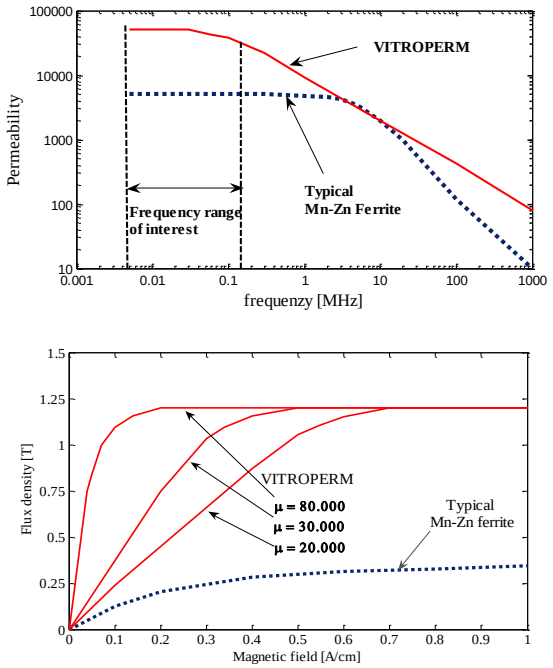

Fig. 8. Magnetization characteristics of the VITROPERM 500F, in comparison with a typical Mn-Zn ferrite (upper) and frequency response of VITROPERM permeability in comparison with a typical Mn-Zn ferrite (lower).

TABLE II.
COMPARISON OF DIFFERENT MAGNETIC CORES CHARACTERISTICS.

Parameter	Symbol	Ferrite N30	VITROPERM 500F
Toroidal core size		50x30x20 mm	25x16x10 mm
Volume	V	50 cm^3	6.25 cm^3
A_L value	A_L	8700 nH,10 kHz	65.5µH, 10 kHz
Saturation flux density	Bs	0.45 T	1.2 T
Weight		114 g	20 g

B. Some considerations on magnetic core saturation

In order to obtain an effective attenuation by the CM choke, the magnetic cores, for both materials, have been accurately chosen. In particular, both geometrical dimensions and magnetic properties of the material have been appropriately selected so to prevent magnetic saturation.

The design criterion for the magnetic core selection is based on the following analysis.

The maximum flux density (B_{max}) in the CM choke magnetic core depends on the flowing peak current in its inductors. If L_1 and L_2 are the inductance of the two windings of the CM choke and M the mutual one, the currents flowing on such inductors are respectively ($I_{DM}+I_{CM}$) and ($-I_{DM}+I_{CM}$).

The magnetic flux due to each of the two windings of the CM choke is given by:

$$\begin{aligned}\phi_1 &= L_1\cdot(I_{DM}+I_{CM})+M\cdot(-I_{DM}+I_{CM})= \\ &=(L_1-M)\cdot I_{DM}+(L_1+M)\cdot I_{CM}\end{aligned} \tag{13}$$

$$\begin{aligned}\phi_2 &= L_2\cdot(-I_{DM}+I_{CM})+M\cdot(I_{DM}+I_{CM})= \\ &=(-L_2+M)\cdot I_{DM}+(L_2+M)\cdot I_{CM}\end{aligned} \tag{14}$$

Therefore, as an upper limit, the overall flux on the core is given by:

$$\phi_{tot}=\phi_1+\phi_2=(L_1-L_2)\cdot I_{DM}+(L_1+L_2+2M)\cdot I_{CM} \tag{15}$$

The term proportional to the DM current is tied to the leakage flux. Moreover, having a coupling factor $k=\frac{M}{\sqrt{L_1L_2}}$ close to unity, the following approximation can be done: $M=L_1=L_2$, where $L_1=L_2$=1.6mH.

Equation (15) can be rewritten as follows:

$$\phi_{tot}=L_{leakage}\cdot I_{DM}+(4L_1)\cdot I_{CM}=L_{leakage}\cdot I_{DM}+4L_1\cdot I_{CM} \tag{16}$$

where:

$$L_{leakage}=(0.1\div 2)\%L_{CM}=(0.8\div 16)\mu H$$

The time domain measurements give the following values of the maximum instantaneous of CM and DM currents respectively:
I_{CM_max}=32 mA e I_{DM_max}=218 mA .

Therefore, the maximum value of the magnetic flux in the core is obtained:

$$\begin{aligned}\phi_{tot\_max} &= (0.8\div 16)\cdot 10^{-6}\cdot 218\cdot 10^{-3}+4\cdot 1.6\cdot 10^{-3}\cdot 32\cdot 10^{-3}= \\ &=(174.4\div 3488)\cdot 10^{-9}+204.8\cdot 10^{-6}\approx 208\cdot 10^{-6}\quad Wb\end{aligned}$$

Moreover the maximum flux can be expressed as:

$$\phi_{tot\_max}=B_{max}\cdot S\cdot N \tag{17}$$

where N is the total number of turns of the windings, S is the cross section of the magnetic core, B_{max} is the maximum value of the magnetic flux density.

On the basis of (17), the maximum magnetic flux density on the core is calculated both in the case of vitroperm and in the case of ferrite material.

The following values of maximum magnetic flux density are obtained for the chosen toroidal cores:

$$\begin{aligned}B_{\max\_vitroperm} &= \frac{\phi_{tot\_\max}}{(h\cdot(r_{out}-r_{\text{int}}))\cdot N}= \\ &=\frac{208\cdot 10^{-6}H\cdot A}{89.375\cdot 10^{-6}m^2\cdot 10}=0.23\text{T}\end{aligned} \tag{18}$$

$$\begin{aligned}B_{\max\_ ferrite} &= \frac{\phi_{tot\_\max}}{(h\cdot(r_{out}-r_{\text{int}}))\cdot N}= \\ &=\frac{208\cdot 10^{-6}H\cdot A}{200\cdot 10^{-6}m^2\cdot 24}=0.043\text{T}\end{aligned} \tag{19}$$

where h, r_{out} and r_{int} are the height, the outer radius and the inner radius of the toroidal cores, respectively.

By considering the variation of the saturation value with the temperature [22], it is possible to find that:

$$0.3\,T(600°C)\le B_{sat\_vitroperm}\le 1.2\,T(20°C) \tag{20}$$

$$0.1\,T(130°C)\le B_{sat\_ferrite}\le 0.38\,T(25°C) \tag{21}$$

Therefore, it is demonstrated that the chosen cores, at the operating temperatures (evaluated by an infrared thermometer, i.e., FLUKE Model 65, and always lower than 130°C), are not affected by magnetic saturation problems.

C. Experimental set-up and performance evaluation

The CM chokes set up with ferrite and VITROPERM cores respectively are shown in Fig. 9. The size reduction with the use of nanocrystalline material is evident. Table III summarizes the features of the EMI filter set up with a CM choke based on the nanocrystalline magnetic core. Fig. 10 shows the prototype of the realized EMI filter. Figs. 11 and 12 show the CM and DM EMI emissions without any filter and with the realized EMI filters. Both CM and DM modes are strongly attenuated. It is worth noting that the DM low frequency performance of the filter using a ferrite core are better due to the higher leakage inductance with respect to the case of vitroperm core.

In Fig. 13 the EMI filter performance are finally shown by comparing the EMI emission of the motor drive, without any filter and with the filtered EMI emission. It is possible to observe that the input EMI filter satisfies the standard limits in the whole frequency range, whereas the use of a nanocrystalline core allows the CM choke size to be

reduced of about 87.5% in volume respect to the use of a ferrite core. Similarly, a reduction of the CM choke weight of 82.5% is obtained.

Fig. 13 shows that the performance of the EMI filter using nanocrystalline core for the CM choke is comparable with that of an EMI filter where the CM choke is realized by using the ferrite core.

Fig. 9. CM choke set up by using an N30 ferrite core (left) and a VITROPERM core (right).

TABLE III.
EMI FILTER FEATURES.

EMI filter parameters					
Parameter	***Value***	***Material***	***Core dimensions mm x mm x mm***	A_L	***N° of turns per winding***
L_{CM}	0.8mH	Vitroperm 500F	25x16x10	65.5µH	5
C_{CM}	200nF	ceramic			
L_{DM}	1.6µH	Leakage (0.2%L_{CM})			
C_{DM}	47µF	electrolytic			

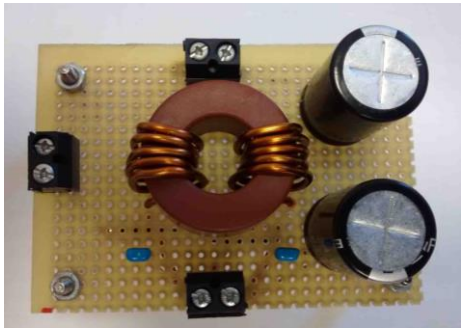

Fig. 10. Pictures of the realized EMI filter.

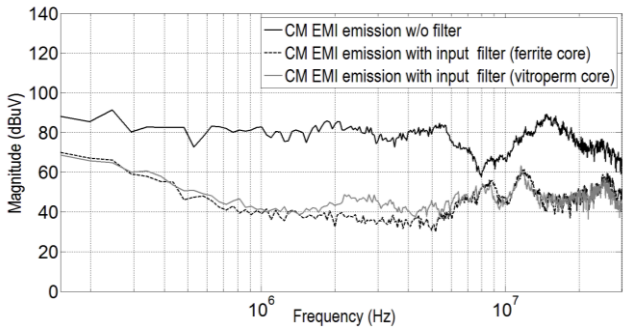

Fig. 11. Measured CM EMI emission without and with EMI filter.

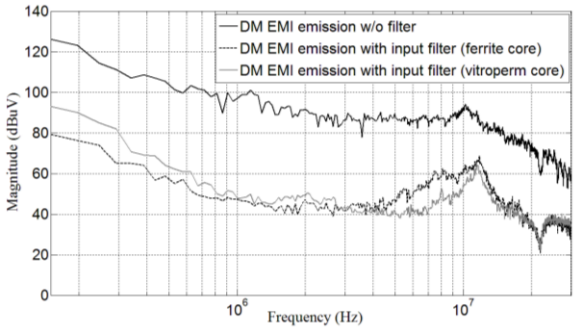

Fig. 12. Measured DM EMI emission without and with EMI filter.

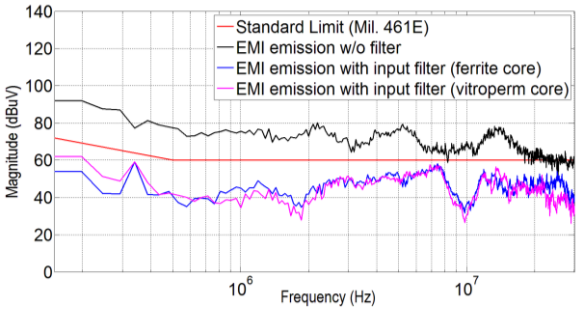

Fig. 13. Measured EMI emission without and with EMI filter.

VII. CONCLUSIONS

A high power density EMI filter design procedure for low voltage-high current induction motor drives, intended for vehicle applications is presented. A software-based CM/DM separation technique is used aiming to simplify the design of the filter and to optimize its size. The proposed method is based on time domain measurements of CM and DM noise by a multi-channel DSO and on their processing via a DFFT algorithm. The software-based CM/DM separation technique as is known is a reliable and cost-effective method in assisting the design of the EMI filters that does not imply the use of expensive RF laboratory equipment or any other dedicated hardware; in addition its usefulness to optimize the power density has been demonstrated. The validation of the proposed technique has been done by comparing the results with those obtained by measurements coming from a high bandwidth RF current probe and a spectrum analyzer. Furthermore the deviation of the results obtained by the two techniques has been computed in terms of NRMSE and NAVE indices: a good agreement has been obtained. Once the effectiveness of the separation technique has been proven, the obtained CM and DM noise levels have been used to design the EMI filter for the motor drive under study. The filter has been set up according to a high power density concept by using a high permeability nano-crystalline magnetic material for the CM choke core which allows a volume reduction of 87.5% and a weight reduction of 82.5%. Finally, experimental tests have demonstrated the good performance of the realized EMI filter.

REFERENCES

[1] G. L. Skibinski, R. J. Kerkman, D. W. Schlegel, “EMI Emissions of Modern PWM AC Drives”, IEEE Ind. Electron. Magaz., Nov./Dec.1999 pp.47-81.

[2] G. Ala, M. C. Di Piazza, A. Ragusa, F. Viola, G. Vitale, “EMI analysis in Electrical Drives Under Lightning Surge Conditions”, IEEE Transactions on Electromagnetic Compatibility, vol 54, no. 4, pp. 850 - 859, 2012.

[3] C. Choochuan, "A Survey of Output Filter Topologies to Minimize the Impact of PWM Inverter Waveforms on Three-Phase AC Indiction Motors" 7th Intern. Pow. Engin. Conf., 2005, IPEC 2005, 29 Nov.-2 Dec. 2005 pp.1-6.

[4] Yoann Y. Maillet, "High-Density Discrete Passive EMI Filter Design for Dc-Fed Motor Drives", Master Thesis, Dept. of Elect. Eng., Virginia Polytechnic Institute and State University, Blacksburg, VA, 2008.

[5] M. C. Di Piazza, G. Giglia, M. Luna, G. Vitale, "EMI and reliability improvement in DC-fed induction motor drives by filtering techniques", 39th Annual Conf. on IEEE Ind. Electron. Society, 2013, pp. 2765-2770.

[6] A. Carrubba, M.C. Di Piazza, G. Tinè, G. Vitale, “Evaluation of common mode disturbance mitigation devices in AC motor drives through HF modelling”, Industrial Electronics, 2006 IEEE International Symposium on 3, pp. 2315-2320.

[7] F.Y. Shih, D.Y. Chen, Y.P. Wu, Y.T. Chen, “A Procedure for Designing EMI Filters for AC Lines Applications”, IEEE Transactions on Power Electronics, vol 11, no. 1, pp.170 - 181, 1996.

[8] Y. Maillet, Rixin Lai, Shuo Wang, Fei Wang, R. Burgos, D. Boroyevich, “High-Density EMI Filter Design for DC-Fed Motor Drives”, IEEE Transactions on Power Electronics, vol. 25, no. 5, May 2010.

[9] J. Biela et al., “Passive and Active Hybrid Integrated EMI Filters”, IEEE Transaction on Power Electronics, vol.24, no.5, May 2009, pp. 1340-1349.

[10] Fang Luo, R. Robutel ,Shuo Wang, Fred Wang, D. Boroyevich, “Integrated Input EMI Filter for a 2 kW DC-fed 3-phase Motor Drive”, Twenty-Fourth Annual IEEE Applied Power Electronics Conference and Exposition, 2009. APEC 2009, pp.325-329.

[11] C. R. Paul, “Introduction to Electromagnetic Compatibility”, Wiley & Sons, 2006.

[12] S. Wang, F.C. Lee, W.G. Odendaal, "Characterization, Evaluation, and Design of Noise Separator for Conducted EMI Noise Diagnosis", IEEE Transactions on Power Electronics, vol 20, no. 4, pp. 974 - 982, July 2005.

[13] M. Kumar, V. Agarwal, "Power Line Filter Design for Conductec Electromagnetic Interference Using Time-Domain Measurements", IEEE Transactions on Power Electronics, vol 48, no. 1, pp. 178 - 186, Feb. 2006.

[14] Y.S. Lee, Y.L. Liang, M.W. Cheng, "Time Domain Measurement System for Conducted EMI and CM/DM Noise Signal Separation", IEEE PEDS 2005.

[15] K. Raggl, T. Nussbaumer, G. Doerig, J. Biela, J. W. Kolar, “Comprehensive Design and Optimization of a High-Power-Density Single-Phase Boost PFC”, IEEE Transactions on Industrial Electronics, vol. 56, no. 7, pp. 2574 - 2587, July 2009.

[16] S. Anand, B. G. Fernandez, “Optimal voltage level for DC microgrids”, in Proc. 36th Annual Conference on IEEE Industrial Electronics Society (IECON 2010), 2010, pp 3034-3039.

[17] R. L. Ozenbaugh, T. M. Pullen, “EMI Filter Design”, III ed., CRC Press, 2012.

[18] Taub, “Principles Of Communication Systems”, McGraw-Hill Education, 2008.

[19] S. Cannizzaro, M.C. Di Piazza, M. Luna, G. Vitale, G. Calogero, I. Citro, “Parameter identification and real-time J-V curve reconstruction of polymer PV and dye-sensitized cells using non-iterative algorithms”, European PV Solar Energy Conference and Exhibition, (EU PVSEC 2014), 22-26 September 2014.

[20] Requirements for the control of electromagnetic interference characteristics of subsystems and equipment, Military Standard 461E, aug. 1999.

[21] SAE AS 1831:1997 (R2010) Characteristics And Utilization Of Electrical Power, 270 V DC, Aircraft.

[22] Vitroperm EMC Products online available online: http://www.vacuumschmelze.com/fileadmin/Medienbiliothek_2010/Downloads/KB/Vitroperm_EMV_EN_full.pdf.